

Observation of Terahertz Radiation via the Two-Color Laser Scheme with Uncommon Frequency Ratios

L.-L. Zhang,¹ W.-M. Wang,^{2,1,*} T. Wu,³ R. Zhang,³ S.-J. Zhang,³
C.-L. Zhang,¹ Y. Zhang,¹ Z.-M. Sheng,^{4,5,6} and X.-C. Zhang^{7,1}

¹*Beijing Advanced Innovation Center for Imaging Technology and Key Laboratory of Terahertz Optoelectronics (MoE),
Department of Physics, Capital Normal University, Beijing 100048, China*

²*Beijing National Laboratory for Condensed Matter Physics,
Institute of Physics, CAS, Beijing 100190, China*

³*Beijing Key Laboratory for Precision Optoelectronic Measurement Instrument and Technology,
School of Optoelectronics, Beijing Institute of Technology, Beijing 100081, China*

⁴*SUPA, Department of Physics, University of Strathclyde, Glasgow G4 0NG, United Kingdom*

⁵*Key Laboratory for Laser Plasmas (MoE) and School of Physics and Astronomy,
Shanghai Jiao Tong University, Shanghai 200240, China*

⁶*IFSA Collaborative Innovation Center, Shanghai Jiao Tong University, Shanghai 200240, China*

⁷*The Institute of Optics, University of Rochester, Rochester, New York 14627, USA*
(Dated: October 20, 2017)

In the widely-studied two-color laser scheme for terahertz (THz) radiation from a gas, the frequency ratio of the two lasers is usually fixed at $\omega_2/\omega_1 = 1:2$. We investigate THz generation with uncommon frequency ratios. Our experiments show, for the first time, efficient THz generation with new ratios of $\omega_2/\omega_1 = 1:4$ and $2:3$. We observe that the THz polarization can be adjusted by rotating the longer-wavelength laser polarization and the polarization adjustment becomes inefficient by rotating the other laser polarization; the THz energy shows similar scaling laws with different frequency ratios. These observations are inconsistent with multi-wave mixing theory, but support the gas-ionization model. This study pushes the development of the two-color scheme and provides a new dimension to explore the long-standing problem of the THz generation mechanism.

Terahertz (THz) waves have broad applications in THz spectroscopy [1, 2] and THz-field matter interactions [3, 4]. These applications can potentially benefit from powerful THz radiation sources with various parameters via different laser-plasma-based schemes [5–9]. For example, MV/cm-scale THz radiation with either linear [5, 10, 11] or elliptical polarization [12–15] can be generated from gas plasma. THz radiation of near mJ can be produced via relativistic laser interaction with solid plasma [8, 16–18]. Among these schemes, the two-color laser scheme [5] has been studied most widely [19–28] because it can provide high-efficiency tabletop broadband sources. Generally, an 800nm pump laser pulse passes through a frequency-doubling crystal to generate a second-harmonic pulse and then the two pulses are mixed to produce gas plasma. Up to now, the frequency ratio of the two-color pulses has been always taken as $\omega_2/\omega_1 = 1:2$ in experiments, although the fundamental-pulse wavelength longer than 800nm was adopted in recent experiments to enhance the THz strength [29–31] and the second-harmonic-pulse frequency was detuned to yield ultra-broadband radiation [32]. Since 2013 a few theoretical reports [33–35] have predicted that the two-color scheme could be extended to uncommon frequency ratios such as $\omega_2/\omega_1 = 1:4, 2:3$, but these predictions have not yet been verified experimentally.

In this Letter, we present the first experimental demonstration of THz generation with uncommon frequency ratios. With the ω_1 -laser wavelength fixed at 800nm and 400nm, respectively, a scan of the ω_2 -laser wavelength

from 1200nm to 1600nm shows that the THz energies have three resonantlike peaks located near $\omega_2/\omega_1 = 1:4, 1:2$, and $2:3$. The energies at these peaks are at the same order. Beyond the previous predictions [33–35], we find that the THz polarization can be adjusted by rotating the ω_2 -pulse polarization and however, the polarization adjustment becomes inefficient by rotating the ω_1 -pulse polarization. In this Letter we define the ω_1 pulse as the higher-frequency one. These observations agree with our particle-in-cell (PIC) simulations and a model based on field ionization.

The current experiments with the new frequency ratios also provide a new dimension to explore further the THz-generation mechanism. Since 2000 it has been a frequently-discussed topic: whether this THz generation can be attributed to multi-wave mixing [5, 10, 36], field ionization [11, 20, 37], or to both [27, 31]. First, multi-wave mixing theory predicts that the THz energy ε_{THz} scales with $(P_1)(P_2)^2$ in the original scheme, where P_1 and P_2 are powers of the two pulses. With $\omega_2/\omega_1 = 1:4$ and $2:3$, ε_{THz} should follow different scaling laws $(P_1)(P_2)^4$ and $(P_1)^2(P_2)^3$, respectively. In the experiments we observe complex dependence of ε_{THz} on P_1 and P_2 similar with different ω_2/ω_1 , in disagreement with these scaling laws. Second, we observe that the THz polarization varies only with rotating the polarization of the longer-wavelength laser, which is inconsistent with the symmetric nature in the susceptibility tensor required by the multi-wave mixing theory [10].

Experimental setup.— Figure 1(a) shows a schematic

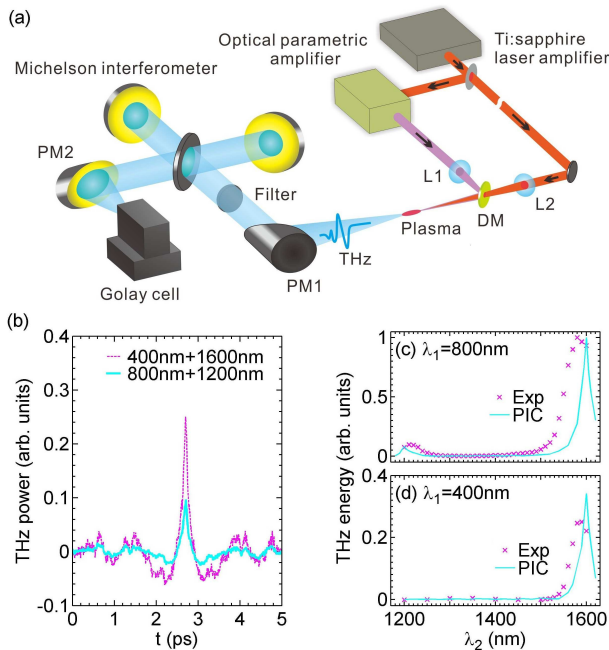


FIG. 1. (a) Experimental setup: L, lens; DM, dichromatic mirror; PM, parabolic mirrors. (b) THz waveforms with $\omega_2/\omega_1 = 1 : 4$ and $2 : 3$, respectively, obtained from the autocorrelation measurements, in which the THz powers are normalized by the one with the 800nm and 1600nm pulses. (c), (d) THz energy as a function of the second pulse wavelength λ_2 , where the first pulse wavelength λ_1 is fixed as 800nm in (c) and 400nm in (d). Powers of the two pulses are taken as $P_1 = 120\text{mW}$ and $P_2 = 400\text{mW}$ in (c) and $P_1 = 180\text{mW}$ and $P_2 = 250\text{mW}$ in (d).

of our experiment. The laser pulse from a Ti:Sapphire amplifier (Spitfire, Spectra Physics) with a central wavelength of 800 nm, duration of 50 fs, and repetition rate of 1 kHz. The pulse with total energy of 5.3 mJ is split into two parts. The part with 3.5 mJ is used to pump an optical parametric amplifier (TOPAS), which delivers a pulse wavelength tunable from 1200 nm to 1600 nm (the ω_2 pulse). The remaining energy is used as the ω_1 pulse of 800 nm wavelength [see Fig. 1(c) as an example]. In another group of experiments [see Fig. 1(d)], the 800 nm pulse passes through a switchable β -barium borate (BBO) crystal and band-pass filter to generate 400nm-wavelength pulse (the ω_1 one). The ω_1 and ω_2 pulses propagate collinearly using a dichromatic mirror and have a confocal spot focused by two convex lenses with equal focal length $f=12.5\text{cm}$. Both pulses are linearly polarized in the horizontal plane initially and their polarizations can be independently controlled by half-wave plates. Powers can also be independently adjusted through optical attenuators. The two pulses irradiate air and produce a few millimeter of plasma.

We use an off-axis parabolic mirror to collect and collimate the forward THz radiation generated from the gas plasma after eliminating the pump laser pulses with

a long-pass THz filter (Tydex Ltd.). To measure the horizontal and vertical components of the radiation, a wire grid polarizer is employed. A Golay THz detector with a 6 mm diameter diamond input window (Microtech SN:220712-D) is used to measure the radiation energy, where the detector shows a nearly flat response in the spectral range from 0.1 THz to 150 THz. The voltage signal is fed into a lock-in amplifier referenced to a 15 THz modulation frequency. To obtain the THz radiation bandwidth, autocorrelation measurement is carried out by a Michelson interferometer containing a silicon wafer.

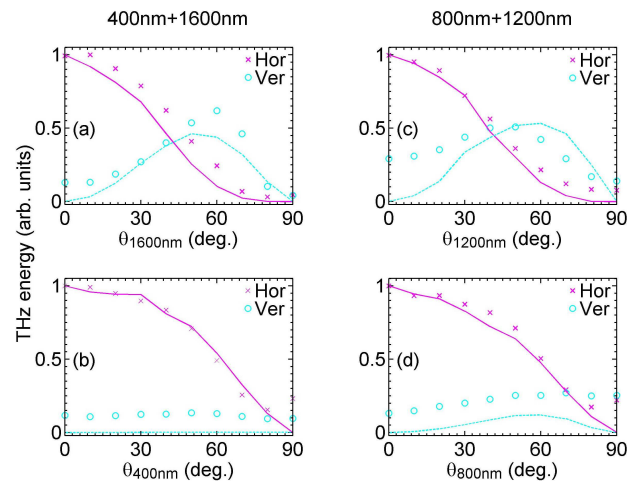


FIG. 2. THz energies of the horizontal and vertical components as a function of the rotation angle θ of the field polarization of (a) the 1600nm pulse, (b) 400nm pulse, (c) 1200nm pulse, and (d) 800nm pulse, respectively, where when polarization of one pulse is rotated, polarization of the other pulse is fixed at the horizontal. Experimental results are shown by crosses and circles and PIC results by lines. The left column corresponds to the case with the 400 nm (with 180mW) and 1600nm (250mW) pulses and the right to the case with the 800nm (120mW) and 1200nm (400mW) pulses.

Experimental and PIC-simulation results.— We first present the experimental and PIC simulation results and then explain them with a theoretical model based on field ionization of gas. In our experiments, we observe dependence of THz generation upon ω_2/ω_1 , laser polarization, and laser power, respectively, as shown in Figs. 1(b)-3. In these figures except Fig. 1(b), our PIC simulation results are also shown. First, the measured THz waveforms plotted in Fig. 1(b) show that the THz peak powers with $\omega_2/\omega_1 = 1 : 4$ and $2 : 3$ are about 30% and 10% compared with $\omega_2/\omega_1 = 1 : 2$. By scanning ω_2 from 1200 nm to 1600 nm, we observe that the THz radiation can be effectively generated only around $\omega_2/\omega_1 = 2 : 3$ and $1 : 2$ in Fig. 1(c) with the ω_1 pulse of 800 nm as well as around $\omega_2/\omega_1 = 1 : 4$ in Fig. 1(d) with the ω_1 pulse of 400 nm. Note that these observed THz peaks have small shifts (10 – 20 nm in wavelength) from the ones exactly at $\omega_2/\omega_1 = 1 : 4$, $2 : 3$, and $1 : 2$ obtained in the PIC re-

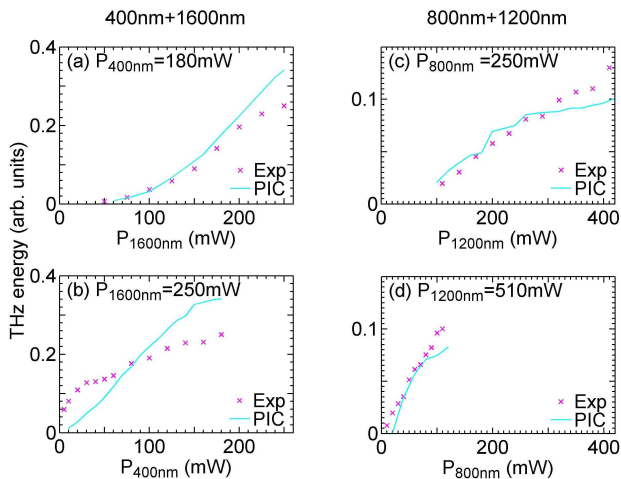


FIG. 3. THz energy as a function of the power of (a) the 1600nm pulse, (b) 400nm pulse, (c) 1200nm pulse, and (d) 800nm pulse, respectively, where when the power of one pulse is changed, the power of the other pulse is fixed. The left column corresponds to the case with the 400nm and 1600nm pulses and the right to the case with the 800nm and 1200nm pulses.

sults, which could be caused by inaccuracy of laser wavelengths output from TOPAS. Second, we observe in Fig. 2 that the THz polarization can be adjusted by rotating the polarization of the ω_2 (longer-wavelength) pulse, but the polarization adjustment becomes inefficient by rotating the ω_1 -pulse polarization. This phenomenon is observed in all the cases of $\omega_2/\omega_1 = 1 : 4$ [Figs. 2(a) and 2(b)], $\omega_2/\omega_1 = 2 : 3$ [Figs. 2(c) and 2(d)], and $\omega_2/\omega_1 = 1 : 2$. For example in the case $\omega_2/\omega_1 = 1 : 4$, when the 1600nm-pulse polarization is rotated from the horizontal to the vertical in Fig. 2(a), the THz horizontal component is first strengthened and then weakened, as observed in previous experiments [30] with $\omega_2/\omega_1 = 1 : 2$. However, when the 400nm-pulse polarization is rotated in Fig. 2(b), the THz vertical component is kept at a low level similar to that at $\theta = 0$ and 90° , which is expected to be at noise level. These observations are reproduced by our PIC simulations. Third, the dependence of the THz energy upon the laser powers does not obey the scaling laws predicted by the multi-wave mixing theory, as seen in Fig. 3. The curves in this figure illustrate complex dependence in both cases $\omega_2/\omega_1 = 1 : 4$ and $2 : 3$ and each curve in the starting phase appears as a linear dependence, in reasonable agreement with the PIC results.

The agreement between the PIC (near-field radiation) and experimental results (far-field radiation) suggests that the far-field radiation observed should be mainly contributed from a short gas-plasma zone in which the pulses have the highest intensities, as modeled in our PIC simulations. In our PIC simulations, we employ a

0.6-millimeter-long nitrogen gas to save computational time. We adopt the same laser parameters as in the experiments and assume that on the front-end of this gas the laser pulses just reach the highest intensities (at the order of 10^{14} W/cm 2) and have the spot radius of $50 \mu\text{m}$. Our PIC simulations are performed with the KLAPS code [38], in which field ionization of gas is realized by Monte Carlo method, movement of the created electrons is computed by the relativistic motion equation, and a full-Maxwell-equation solver is included to calculate generation and propagation of both lasers and radiation. It can self-consistently compute plasma production and net current formation via laser-field ionization, dynamics of the net current in the plasma, and THz generation. Therefore, our PIC simulation can give near-field THz radiation with very few approximations. Note that the far-field radiation is expected to be composed of all near-field sources [23, 24, 28] and a simplified near-field model was used to well explain THz generation experiments in Ref. [30].

Theoretical model.— To interpret the PIC results and the experiment results, we present theoretical analysis based on a net or transient current model. It was first proposed by Kim *et al.* [11, 19] to show current formation due to asymmetric field ionization. Then, Wang *et al.* proposed a near-field model including the current dynamics in plasma [15, 20, 39]. The THz radiation generation includes two processes: net-current formation via field ionization and THz generation as the current is modulated by the plasma. The former lasts a time shorter than the laser duration 50 fs while the latter has a timescale at the THz period about 1 ps. Therefore, one can calculate the two processes respectively. The net current $\mathbf{J}_0 = -en_e\mathbf{v}_0$ can be given by

$$\mathbf{J}_0 = \frac{e^2 n_e \mathbf{A}_L(\psi_0)}{m_e c}, \quad (1)$$

where $\mathbf{v}_0 = -e\mathbf{A}_L(\psi_0)/m_e c$, \mathbf{A}_L is the laser vector potential, $\psi = t - z/c$, and ψ_0 is the position where electrons are created. Note that nearly all electrons are periodically created at the same relative position in different periods of the laser fields in the cases $\omega_2/\omega_1 = 1:4, 1:2, 2:3$, respectively, as shown in Ref. [35]. The electron density is given according to $\partial n_e/\partial t = (n_a - n_e)w(E_L)$, where $w(E_L)$ is the ionization rate [40–42] in the laser field amplitude E_L and n_e and n_a are the electron and initial atom densities, respectively. After passage of the laser pulses, the generated radiation interacts with the current, the electron velocity becomes $\mathbf{v} = \mathbf{v}_0 + e\mathbf{A}_{THz}/m_e c$, and consequently the current turns to $\mathbf{J} = \mathbf{J}_0 - e^2 n_e \mathbf{A}_{THz}/m_e c$, where impacts of the radiation ponderomotive force on n_e can be ignored. Then, the THz radiation can be described by

$$\left[\nabla^2 - \frac{1}{c^2} \frac{\partial^2}{\partial t^2} - \frac{\omega_p^2}{c^2} \right] \mathbf{A}_{THz} = -4\pi \mathbf{J}_0/c, \quad (2)$$

where $\omega_p = \sqrt{4\pi e^2 n_e / m_e}$ is the plasma oscillation frequency. Equation (2) is difficult to analytically solve since the pulse length of the THz radiation is longer than the spot size ($\sim 50\mu\text{m}$) and a one-dimensional approximation [39] cannot be taken. In the following, we will show that numerical calculation of Eq. (1) and simple analysis of Eq. (2) can explain the experimental results presented previously.

Dependence on laser frequency ratio.— From Eqs. (1) and (2), one can obtain the THz amplitude $A_{THz} \propto J_0 \propto A_L(\psi_0)$. Peaks of THz energies appear at peaks of $A_L(\psi_0)$. Our calculation shows three resonance-like peaks of $A_L(\psi_0)$ located at $\omega_2/\omega_1 = 1:4, 1:2, 2:3$. To quantitatively compare the THz energies at the three peaks, we also calculate J_0 which depends on both $A_L(\psi_0)$ and n_e . Calculating J_0 by Eq. (1) gives the values of J_0 as $0.29 : 1 : (-0.58)$. Then, the THz energies are $0.084 : 1 : 0.34$, which is in agreement with the experimental results of $0.097 : 1 : 0.26$ as seen in Figs. 1(c) and 1(d).

Dependence on laser polarization.— According to Eqs. (1) and (2), the THz radiation should have only the x component if the two pulses have the same polarization along the x direction. Once the polarization of one pulse is rotated to have the y component, the radiation could have both x and y components. We take the laser electric fields as $E_{L,x} = f(\psi)[a_1 \sin(\omega_1\psi) + a_2 \cos(\theta) \sin(\omega_2\psi)]$ and $E_{L,y} = f(\psi)a_2 \sin(\theta) \sin(\omega_2\psi)$, where θ is the rotation angle and $f(\psi)$ is the envelope profile. The vector potential can be written by $A_{L,x} = cf(\psi)[a_1 \cos(\omega_1\psi)/\omega_1 + a_2 \cos(\theta) \cos(\omega_2\psi)/\omega_2]$ and $A_{L,y} = cf(\psi)a_2 \sin(\theta) \cos(\omega_2\psi)/\omega_2$ since $\partial f(\psi)/\partial\psi \ll \omega_1$ and ω_2 for the pulse duration of 50 fs. Electrons are created at the maximum of $E_L^2 = f^2(\psi)[a_1^2 \sin^2(\omega_1\psi) + a_2^2 \sin^2(\omega_2\psi) + 2a_1 a_2 \cos(\theta) \sin(\omega_1\psi) \sin(\omega_2\psi)]$, i.e., at $\frac{\partial |E_L|}{\partial\psi} = 0$, which gives $\omega_2\psi_0 = 1.937$ for $\theta = 0$ (a_1 and a_2 are computed from $P_{400nm} = 180$ mW and $P_{1600nm} = 250$ mW, respectively). Our calculation shows that ψ_0 varies slightly with the change in θ , because $\sin(\omega_1\psi)$ and $\sin(\omega_2\psi)$ are close to 1 to produce the maximum of $|E_L|$ with $a_1 \sim a_2$. With $\omega_2\psi_0 = 1.937$, $\partial[\frac{\partial |E_L|}{\partial\psi}]/\partial[\cos(\theta)] \simeq 0.06$ can be derived, which suggests that when $\cos(\theta)$ is changed from 1 to 0 (θ from 0 to $\pi/2$), $\frac{\partial |E_L|}{\partial\psi}|_{\psi_0+\epsilon} = 0$ is always satisfied if ψ_0 is shifted by a small value ϵ .

Therefore, both $|E_L(\psi_0)|$ and $|A_{L,x}(\psi_0)|$ decreases as θ is increased from 0 to $\pi/2$, where $A_{L,x}(\psi_0) < 0$ and $\cos(\omega_2\psi_0) < 0$. Decrease of $|E_L(\psi_0)|$ and $|A_{L,x}(\psi_0)|$ leads to a reduction of ionization rates and net velocities of electrons, respectively, which can explain the weakening THz horizontal (or x) component with θ in Fig. 2(a). This figure also shows that the vertical component is first strengthened from zero and then weakened, which is caused by the increasing $|A_{L,y}(\psi_0)|$ and decreasing $|E_L(\psi_0)|$ with θ . The peak of the vertical component

is observed about $\theta = 60^\circ$ approaching the PIC result. Our simulations show the optimized θ within $40^\circ - 70^\circ$ dependent of the laser intensities and frequencies, determined by the balancing point of the increasing $|A_{L,y}(\psi_0)|$ and the decreasing $|E_L(\psi_0)|$.

In Fig. 2(b) the 400 nm pulse polarization (the ω_1 pulse) is rotated, the THz vertical component is kept at a low level (noise level in the experiments and near zero in the PIC simulations). Rotating the ω_1 or ω_2 pulse, $|E_L|$ is unchanged and consequently, $\frac{\partial |E_L|}{\partial\psi} = 0$ gives the same $\omega_2\psi_0 = 1.937$ for $\theta = 0$ and ψ_0 varies slightly with θ . Therefore, the horizontal component in Fig. 2(b) shows the similar dependence to Fig. 2(a) for the same reason addressed previously. However, the vertical component depends strongly on the laser frequency. When rotating the ω_1 pulse, $A_{L,y}^{\omega_1}(\psi_0) = cf(\psi_0)a_1 \sin(\theta) \cos(\omega_1\psi_0)/\omega_1$. While rotating the ω_2 pulse, $A_{L,y}^{\omega_2}(\psi_0) = cf(\psi_0)a_2 \sin(\theta) \cos(\omega_2\psi_0)/\omega_2$. One can obtain

$$\frac{A_{L,y}^{\omega_1}(\psi_0)}{A_{L,y}^{\omega_2}(\psi_0)} \simeq -\left(\frac{\omega_2}{\omega_1}\right)^2 = -\left(\frac{\lambda_1}{\lambda_2}\right)^2, \quad (3)$$

where we have used $a_1\omega_1 \cos(\omega_1\psi_0) = -a_2\omega_2 \cos(\omega_2\psi_0)$ derived from $\frac{\partial |E_L|}{\partial\psi} = 0$ with $\theta = 0$ since ψ_0 slightly depends upon θ . According to Eq. (3), the THz energy of the vertical component is decreased to $1/256 \simeq 0.004$ when the rotated pulse is changed from the ω_2 one to the ω_1 with $\omega_2/\omega_1 = 1 : 4$; and the THz energy is decreased to $16/81 \simeq 0.2$ with $\omega_2/\omega_1 = 2 : 3$. These are in good agreement with our PIC results as shown in Figs. 2(b) and 2(d). Since such low levels of THz energies cannot be resolved in our experiments, the vertical component is observed to be nearly unchanged with varying θ . Similar results are also observed in our experiments when the 800 nm and 1600 nm pulses are used.

Note that the observed THz polarization dependence is inconsistent with the multi-wave mixing model [10]. For example with $\omega_2/\omega_1 = 1 : 4$, the fifth-order susceptibility tensor χ for THz generation has $\chi_{xyyyy}^x = \chi_{yxxxx}^y$ because of the symmetry, where the superscript of χ represents the THz polarization and the subscripts represent the polarization of the ω_1 wave and the four ω_2 waves, respectively. $\chi_{xyyyy}^x = \chi_{yxxxx}^y$ requires that the horizontal THz component in Fig. 2(a) should have the same level as the vertical THz component in Fig. 2(b). In contrast, Figs. 2(a) and 2(b) gives $\chi_{xyyyy}^x \gg \chi_{yxxxx}^y$. Besides, both our PIC and experimental results show obvious differences from $\cos^2(\theta)$ scaling for the horizontal component and $\sin(2\theta)$ for the vertical component, which was derived under the different condition $a_1 \ll a_2$ and with $\omega_2/\omega_1 = 1 : 2$ [30].

Dependence on laser power.— Figure 3 shows complex dependence of the THz energy on the laser power for $\omega_2/\omega_1 = 1 : 4$ and $2 : 3$, which significantly deviates from the scaling of $(P_1)(P_2)^4$ and $(P_1)^3(P_2)^2$ predicted by the multi-wave mixing theory. This can be

attributed to complex dependence of the ionization rates on the laser intensities since the intensities span one to two orders of magnitude, which adds significant complexity to theoretical analysis. The analysis becomes simpler when the power of one pulse is changed in a low level within $[P_a, P_b]$ and the power of the other pulse is fixed at a much higher value P_c ($P_c \gg P_b$), where the ionization rate and the ionization position ψ_0 vary slightly. This is the case in the starting stage in each curve in Fig. 3. According to $\frac{\partial |E_L|}{\partial \psi}(\psi_0) = 0$ for the two pulses with the same polarization, one can obtain $A_{L,x}(\psi_0) = a_1 c f(\psi_0) \cos(\omega_1 \psi_0) [1/\omega_1 - \omega_1/\omega_2^2]$ or $A_{L,x}(\psi_0) = a_2 c f(\psi_0) \cos(\omega_2 \psi_0) [1/\omega_2 - \omega_2/\omega_1^2]$. In the case with the laser powers $P_1 \gg P_2$ and $P_1 \ll P_2$, ψ_0 varies slightly with the change of a_1 and a_2 and therefore, $|A_{L,x}(\psi_0)|$ is linearly proportional to a_1 or a_2 , i.e., the THz energy is linearly proportional to P_1 or P_2 . This linear dependence is observed within the starting stage in each curve in Fig. 3 with either $\omega_2/\omega_1 = 1:4$ or $2:3$ (one can also observe similar results in previous experiments with $\omega_2/\omega_1 = 1:2$ [30]). Note that the PIC and experimental results are not in precise agreement. In the PIC simulations we assume that the laser pulses with different powers have the same spot radius of $50 \mu m$ when they reach the highest intensities. However, the spot radius will depend on the power, unfortunately, exploration of this complex dependence is beyond the scope of this work.

In summary, we have experimentally shown that the two-color scheme can still work when ω_2/ω_1 of 1:2 is changed to 1:4 and 2:3. The THz polarization can be adjusted more efficiently by rotating the polarization of the longer-wavelength pulse from the horizontal to the vertical because the THz vertical component follows a fourth-power law of the laser wavelength, which is inconsistent with the multi-wave mixing theory. We have observed a complex dependence of the THz energy when the power of one of the two pulses is varied over a large range. A linear dependence with different ω_2/ω_1 has also been observed when the power of one pulse is varied within a limited range much lower than the power of the other pulse. These dependencies disagree with the scaling laws given by the multi-wave mixing theory. These observations have been well explained by our PIC simulations and a model based on field ionization.

This work was supported by the National Basic Research Program of China (Grant No. 2014CB339806 and No. 2014CB339801), the National Natural Science Foundation of China (Grants No. 11375261, No. 11775302, and No. 11374007), Science Challenge Project of China (Grant No. TZ2016005), and the Strategic Priority Research Program of the Chinese Academy of Sciences (Grants No. XDB16010200 and XDB07030300).

-
- * hbwwm1@iphy.ac.cn or weiminwang1@126.com
- [1] B. Clough, J. Dai, and X.-C. Zhang, *Mater. Today* **15**, 50 (2012).
 - [2] P. Gaal, W. Kuehn, K. Reimann, M. Woerner, T. Elsaesser, and R. Hey, *Nature* **450**, 1210 (2007).
 - [3] T. Kampfrath, K. Tanaka, and K. Nelson, *Nat. Photonics* **7**, 680 (2013).
 - [4] S. Spielman, B. Parks, J. Orenstein, D. T. Nemet, F. Ludwig, J. Clarke, P. Merchant, and D. J. Lew, *Phys. Rev. Lett.* **73**, 1537 (1994).
 - [5] D. J. Cook and R. M. Hochstrasser, *Opt. Lett.* **25**, 1210 (2000).
 - [6] C. D'Amico, A. Houard, M. Franco, B. Prade, A. Mysyrowicz, A. Couairon, and V. T. Tikhonchuk, *Phys. Rev. Lett.* **98**, 235002 (2007).
 - [7] Z.-M. Sheng, K. Mima, J. Zhang, and H. Sanuki, *Phys. Rev. Lett.* **94**, 095003 (2005).
 - [8] A. Gopal, S. Herzer, A. Schmidt, P. Singh, A. Reinhard, W. Ziegler, D. Brommel, A. Karmakar, P. Gibbon, U. Dillner et al., *Phys. Rev. Lett.* **111**, 074802 (2013).
 - [9] Z. Jin, Z. L. Chen, H. B. Zhuo, A. Kon, M. Nakatsutsumi, H. B. Wang, B. H. Zhang, Y. Q. Gu, Y. C. Wu, B. Zhu, L. Wang, M. Y. Yu, Z. M. Sheng, and R. Kodama, *Phys. Rev. Lett.* **107**, 265003 (2011).
 - [10] X. Xie, J. Dai, and X.-C. Zhang, *Phys. Rev. Lett.* **96**, 075005 (2006).
 - [11] K. Y. Kim, J. H. Glowina, A. J. Taylor and G. Rodriguez, *Opt. Express* **15**, 4577 (2007).
 - [12] H. C. Wu, J. Meyer-ter-Vehn, and Z. M. Sheng, *New J. Phys.* **10**, 043001 (2008).
 - [13] J. Dai, N. Karpowicz, and X.-C. Zhang, *Phys. Rev. Lett.* **103**, 023001 (2009).
 - [14] H. Wen and A. M. Lindenberg, *Phys. Rev. Lett.* **103**, 023902 (2009).
 - [15] W.-M. Wang, P. Gibbon, Z.-M. Sheng, and Y.-T. Li, *Phys. Rev. Lett.* **114**, 253901 (2015).
 - [16] G. Q. Liao, Y. T. Li, C. Li, L. N. Su, Y. Zheng, M. Liu, W. M. Wang, Z. D. Hu, W. C. Yan, J. Dunn, J. Nilsen, J. Hunter, Y. Liu, X. Wang, L. M. Chen, J. L. Ma, X. Lu, Z. Jin, R. Kodama, Z. M. Sheng, and J. Zhang, *Phys. Rev. Lett.* **114**, 255001 (2015).
 - [17] G.-Q. Liao, Y.-T. Li, Y.-H. Zhang, H. Liu, X.-L. Ge, S. Yang, W.-Q. Wei, X.-H. Yuan, Y.-Q. Deng, B.-J. Zhu, Z. Zhang, W.-M. Wang, Z.-M. Sheng, L.-M. Chen, X. Lu, J.-L. Ma, X. Wang, and J. Zhang, *Phys. Rev. Lett.* **116**, 205003 (2016).
 - [18] Z. Jin, H. B. Zhuo, T. Nakazawa, J. H. Shin, S. Wakamatsu, N. Yugami, T. Hosokai, D. B. Zou, M. Y. Yu, Z. M. Sheng, and R. Kodama, *Phys. Rev. E* **94**, 033206 (2016).
 - [19] K. Y. Kim, A. J. Taylor, J. H. Glowina, and G. Rodriguez, *Nat. Photonics* **2**, 605 (2008).
 - [20] W.-M. Wang, Z.-M. Sheng, H.-C. Wu, M. Chen, C. Li, J. Zhang, and K. Mima, *Opt. Express* **16**, 16999 (2008).
 - [21] Y. Chen, T.-J. Wang, C. Marceau, F. Theberge, M. Chateaufneuf, J. Dubois, O. Kosareva and S. L. Chin, *Appl. Phys. Lett.* **95**, 101101 (2009).
 - [22] T.-J. Wang, Y. Chen, C. Marceau, F. Theberge, M. Chateaufneuf, J. Dubois, and S. L. Chin, *Appl. Phys. Lett.* **95**, 131108 (2009).
 - [23] I. Babushkin, W. Kuehn, C. Kohler, S. Skupin, L. Berge,

- K. Reimann, M. Woerner, J. Herrmann, and T. Elsaesser, *Phys. Rev. Lett.* **105**, 053903 (2010).
- [24] I Babushkin, S Skupin, A Husakou, C Kohler, E Cabrera-Granado, L Berge and J Herrmann, *New J. Phys.* **13**, 123029 (2011).
- [25] Y. S. You, T. I. Oh, and K. Y. Kim, *Phys. Rev. Lett.* **109**, 183902 (2012).
- [26] P. Gonzalez de Alaiza Martinez, I. Babushkin, L. Berge, S. Skupin, E. Cabrera-Granado, C. Kohler, U. Morgner, A. Husakou, and J. Herrmann, *Phys. Rev. Lett.* **114**, 183901 (2015).
- [27] V. A. Andreeva, O. G. Kosareva, N. A. Panov, D. E. Shipilo, P. M. Solyankin, M. N. Esaulkov, P. Gonzalez de Alaiza Martinez, A. P. Shkurinov, V. A. Makarov, L. Berge, and S. L. Chin, *Phys. Rev. Lett.* **116**, 063902 (2016).
- [28] Z. Zhang, Y. Chen, M. Chen, Z. Zhang, J. Yu, Z. Sheng, J. Zhang, *Phys. Rev. Lett.* **117**, 243901 (2016).
- [29] M. Clerici, M. Peccianti, B. E. Schmidt, L. Caspani, M. Shalaby, M. Giguere, A. Lotti, A. Couairon, F. Legare, T. Ozaki, D. Faccio, and R. Morandotti, *Phys. Rev. Lett.* **110**, 253901 (2013).
- [30] N. V. Vvedenskii, A. I. Korytin, V. A. Kostin, A. A. Murzanev, A. A. Silaev, and A. N. Stepanov, *Phys. Rev. Lett.* **112**, 055004 (2014).
- [31] L. Berge, S. Skupin, C. Kohler, I. Babushkin, and J. Herrmann, *Phys. Rev. Lett.* **110**, 073901 (2013).
- [32] M. D. Thomson, V. Blank, and H. G. Roskos, *Opt. Express* **18**, 23173 (2010).
- [33] W.-M. Wang, Y.-T. Li, Z.-M. Sheng, X. Lu, and J. Zhang, *Phys. Rev. E* **87**, 033108 (2013).
- [34] V. A. Kostin, I. D. Laryushin, A. A. Silaev, and N. V. Vvedenskii, *Phys. Rev. Lett.* **117**, 035003 (2016).
- [35] W.-M. Wang, Z.-M. Sheng, Y.-T. Li, Y. Zhang, and J. Zhang, *Phys. Rev. A* **96**, 023844 (2017).
- [36] K. Liu, A. D. Koulouklidis, D. G. Papazoglou, S. Tzortzakis, and X.-C. Zhang, *Optica* **3**, 605 (2016).
- [37] D. Zhang, Z. Lu, C. Meng, X. Du, Z. Zhou, Z. Zhao, and J. Yuan, *Phys. Rev. Lett.* **109**, 243002 (2012).
- [38] W.-M. Wang, P. Gibbon, Z.-M. Sheng, and Y.-T. Li, *Phys. Rev. E* **91**, 013101 (2015).
- [39] W.-M. Wang, S. Kawata, Z.-M. Sheng, Y.-T. Li, and J. Zhang, *Phys. Plasmas* **18**, 073108 (2011).
- [40] M. V. Ammosov, N. B. Delone, and V. P. Krainov, *Sov. Phys. JETP* **64**, 1191 (1986).
- [41] B. M. Penetrante and J. N. Bardsley, *Phys. Rev. A* **43**, 3100 (1991).
- [42] G. Gibson, T. S. Luk, and C. K. Rhodes, *Phys. Rev. A* **41**, 5049 (1990).